Non-Gaussian anomalous diffusion of optical vortices

Jiaxing Gong,[1] Qi Li,[1] Shaoqun Zeng,[2] and Jing Wang[1,*]

[1]*Department of Biomedical Engineering, College of Life Science and Technology, Huazhong University of Science and Technology, Wuhan 430074, China*

[2]*Britton Chance Center for Biomedical Photonics, Wuhan National Laboratory for Optoelectronics, MoE Key Laboratory for Biomedical Photonics, School of Engineering Sciences, Huazhong University of Science and Technology, Wuhan 430074, China*

(Received 11 July 2023; accepted 15 December 2023; published 14 February 2024)

Anomalous diffusion of different particlelike entities, the deviation from typical Brownian motion, is ubiquitous in complex physical and biological systems. While optical vortices move randomly in evolving speckle fields, optical vortices have only been observed to exhibit pure Brownian motion in random speckle fields. Here we present direct experimental evidence of the anomalous diffusion of optical vortices in temporally varying speckle patterns from multiple-scattering viscoelastic media. Moreover, we observe two characteristic features, i.e., the self-similarity and the antipersistent correlation of the optical vortex motion, indicating that the mechanism of the observed subdiffusion of optical vortices can only be attributed to fractional Brownian motion (FBM). We further demonstrate that the vortex displacements exhibit a non-Gaussian heavy-tailed distribution. Additionally, we modulate the extent of subdiffusion, such as diffusive scaling exponents, and the non-Gaussianity of optical vortices by altering the viscoelasticity of samples. The discovery of the complex FBM but non-Gaussian subdiffusion of optical vortices may not only offer insight into certain fundamental physics, including the anomalous diffusion of vortices in fluids and the decoupling between Brownianity and Gaussianity, but also suggest a strong potential for utilizing optical vortices as tracers in microrheology instead of the introduced exogenous probe particles in particle tracking microrheology.

DOI: 10.1103/PhysRevE.109.024111

I. INTRODUCTION

Brownian motion or normal diffusion of particles is the most fundamental stochastic process that has kept arousing new physics and renewed interests across many disciplines for over a century since the celebrated works of Einstein, Langevin, and Smoluchowski [1]. Brownian motion is defined by two characteristic features: the linear increase with time of the mean-square displacement (MSD) and the Gaussian distribution of the probability density function (PDF) of particle displacements. Deviations from one or both of the two features are also common. Anomalous diffusion characterized by the power-law growth of the MSD $\langle \Delta r^2(\tau) \rangle \sim \tau^\alpha$ with $\alpha \neq 1$ has been widely demonstrated in different physical and biological systems. Subdiffusion with $0 < \alpha < 1$ has been observed for particles in crowded environments, like nanoparticles in the cytoplasm of biological cells, and particles diffusing in porous material [2,3]. Superdiffusion with $\alpha > 1$ has been demonstrated for active molecular-motor-driven motion in biological cells, animals searching for food, and vortices in quantum fluids [4–6]. The two features of Brownian motion were thought to be strictly linked until the discovery of the so-called Fickian yet non-Gaussian diffusion (FNGD), just over a decade ago [7–11]. In FNGD, the linear time dependence of the MSD (Fickian) coexists with a non-Gaussian PDF of displacements for given time lags.

The most fundamental and simplest Brownian system is the isolated spherical particles with certain mass and size in an incompressible fluid with density and viscosity. Normal and anomalous diffusion have been discovered for varied particlelike entities, including atoms [12], colloid [13], molecules [1], and cell organelles [14]. However the diffusion phenomena are not solely limited to the particles with mass and size; they also encompass the massless or topological objects in various systems. Examples include singular points in phase fields of matter or electrical waves, such as fluid vortices [15,16], and topological defects of matter or bioelectrical waves in living systems [17–19]. The properties and evolution of these singular points play a critical role in understanding the function and internal structure of complex systems [20,21].

Optical vortices, the singular points in random optical wave fields, are also performing particlelike random-looking motion in fluctuating random fields. By recognizing the analogy between complex fluids and random wave fields [22,23], different hydrodynamic features, such as vortex rotation and interaction between a few neighboring vortices, have been discovered for optical vortices [24–28]. The dynamic behaviors of optical vortices have been widely utilized to characterize the physical and dynamic properties of complex systems [22,29–32]. For instance, velocity statistics have been proposed to serve as a measure of wave localization in strong scattering random media [31]. The displacement information of optical vortices is a sensitive assessment of nanometric displacements or deformation of a sample, and the photon diffusion coefficient through the random medium [33–35]. Optical vortex tracking has also been applied to evaluate tissue

*wang.jing@hust.edu.cn

viscoelasticity, track cellular movement, and assess microcirculation [36–38]. However, despite substantial advances in understanding and applying optical vortex stochastic motion, only the pure Brownian diffusion of optical vortices has been reported [35,39–41]. The anomalous diffusion of optical vortices has not been demonstrated yet, let alone the underlying physical mechanism.

In this paper we report our experimental observations of the non-Gaussian anomalous diffusion of optical vortices in dynamic speckles and reveal the underlying mechanisms of the anomalous diffusion of the optical vortices. Since the phase of fast-varying speckle fields is challenging to acquire in experiments, we apply the Laguerre-Gauss (LG) transformation to the speckle intensity pattern recorded by a high-speed camera. The phase of the corresponding complex representation generated from the LG transformation is what we designate as the pseudophase. We subsequently verify through numerical simulation that the motion of optical vortices in both the pseudophase and the real phase is consistent. This is demonstrated by showing that various statistical measures, such as MSD and velocity correlation of the optical vortex motion in the pseudophase, are strictly identical to those of the optical vortices in the real phase. Therefore, in the experiment, we employ the motion statistics of optical vortices in the pseudophase to represent the motion statistics of optical vortices in the real phase. Experimentally, we acquire sequences of dynamic speckle patterns from the multiple-scattering polydimethylsiloxane (PDMS) sample during the entire process of PDMS gelation. We investigate the collective motion of optical vortices in the pseudophase calculated via the LG transformation to the speckle patterns and we find that the optical vortices perform a typical subdiffusive behavior, the power-law temporal increase of MSD, $\langle \Delta r^2(\tau) \rangle \sim \tau^\alpha$, with $0 < \alpha < 1$. We next model the vortex subdiffusive behavior with fractional Brownian motion (FBM), a Gaussian process commonly used to model particle diffusion in a viscoelastic environment. In addition, we observe a robust non-Gaussian behavior in the probability distribution of the vortex displacements. Moreover, we tune the degree of subdiffusion of the optical vortex by modifying the viscoelasticity of the sample, suggesting that the optical vortices may serve as surrogate probes in optical microrheology for turbid media [42]. The extensive study of the diffusive motion of optical vortices may not only enrich our understanding of the optical vortex diffusion in speckle fields, but also contribute to further investigations of a variety of fundamental physical phenomena, including wave transport in disordered media [26], turbulent diffusion in quantum fluids [22,43], and the riddle of anomalous yet non-Gaussian diffusion [44].

II. MATERIALS AND METHODS

Optical vortices, or phase singularities, in speckle fields are defined as intensity nulls where both the real and imaginary parts of the fields vanish. All equiphase lines of speckle fields converge to the phase singularities as shown in Fig. 1(a). The accumulated phase change along with a contour surrounding a single vortex is integer times of 2π, $q = \frac{1}{2\pi} \oint \vec{\nabla}\varphi(x, y) \cdot d\vec{l}$, where the nonzero, signed integer q is referred to as the topological charge of the vortex. Only optical vortices with topological charge ± 1 can stably exist in random speckle fields [45]. High-order vortices are unstable and thus their occurrence is improbable in speckle fields [46–48]. The optical vortices with opposite topological charge always appear and disappear in pairs [49,50]. The optical vortices connected by equiphase lines form a network spreading over the whole speckle field and determine the skeleton structure of random wave fields, as shown in Fig. 1(a). All these described features of optical vortices can help us determine the precise locations of vortices in speckles [31,42,51].

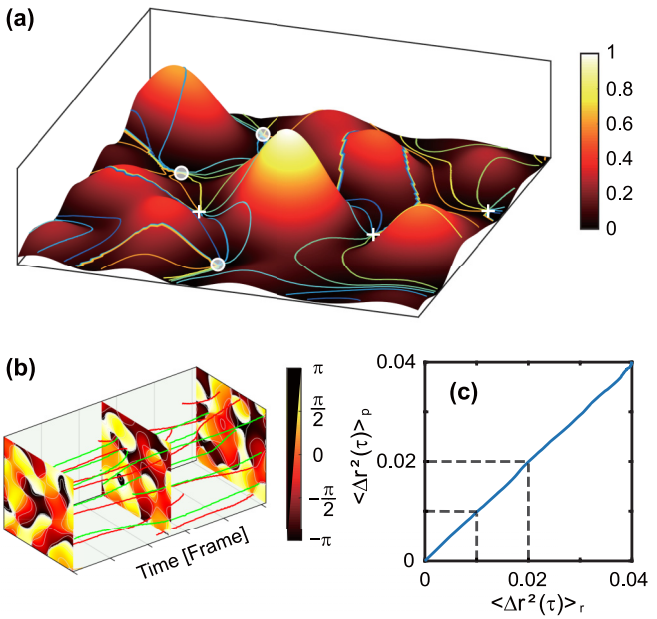

FIG. 1. Optical vortices in the speckle field. (a) Optical vortices occur at intensity nulls and the intersections of phase contours (solid lines). The phase difference between each equiphase line is $\pi/4$. The value of the normalized speckle intensity is represented by the color defined in the color bar. (b) Random motion of optical vortices in the numerically generated dynamic speckle fields. The red lines and green lines represent the trajectories of the positive and negative optical vortices, respectively. (c) Linear correlation between the MSD of optical vortices in the real phase and the pseudophase.

The collective motion of optical vortices in temporally varying speckle fields can be revealed by analyzing the lifelong trajectories of the optical vortices [52]. We follow the trajectories by locating, distinguishing, and linking the phase singularities in sequential speckle patterns according to the definition and the morphological features of optical vortices [33,42,53]. We determine the position of an optical vortex by unwrapping the phase change along a closed counterclockwise contour around the vortex. The accumulated phase change around a single vortex is $\pm 2\pi$, corresponding to the topological charge of ± 1. The locations of the identified vortices over multiple frames trace a distinct vortex trail. The criterion of the new trail and existing trail is determined by the spatial correlation of speckles, or average speckle size. The vortex trajectories are then followed from creation to annihilation, as shown in Fig. 1(b). The optical vortex tracking algorithm remains identical for the real phase and pseudophase of speckle fields in simulations and the pseudophase of speckle intensity patterns in experiments.

A. Complex representations of speckle intensity patterns

In order to locate and track optical vortices or phase singularities in dynamic speckles, accurate phase information of speckle fields is essential. To acquire or recover the phase of the fast-varying laser speckle fields is an arduous task due to the considerable complications of experiments and algorithms. Digital holography or digital speckle-pattern interferometry are typical techniques that can be used to reconstruct the phase map of speckle fields [54,55]. However, these techniques are only capable of recovering real phase maps without singular structures or the phase with at most only a few singularities [56]. Complex speckle fields usually maintain a high spatial density of optical vortices since there is one vortex for every speckle grain on average [57]. In particular, when the nucleation or annihilation of two optical vortices with opposite topological charges happens, the separate distance between the vortices may be extremely small, making it difficult to distinguish these optical vortices in the interferometric phase measurements [58]. Therefore, it is challenging for us to investigate the collective motion of optical vortices by recovering the real phase of speckle fields experimentally with these interferometric methods.

In the fields of physics, it is a prevailing practice to represent real-valued signals by their corresponding complex-valued counterparts [59]. Here we construct the complex signal representation of the input speckle by applying the LG transformation to the speckle intensity as [53,60–62]

$$\begin{aligned}\tilde{E}(x,y) &= |\tilde{A}(x,y)|\exp[j\tilde{\varphi}(x,y)] \\ &= \iint \mathcal{T}_{\mathrm{LG}}(f_x,f_y)\mathcal{F}(f_x,f_y) \\ &\quad \times \exp[j2\pi(f_x x + f_y y)]df_x df_y, \end{aligned} \tag{1}$$

where $\mathcal{F}(f_x, f_y)$ is the Fourier spectrum of speckle intensity $I(x, y)$, and $\tilde{A}(x, y)$ and $\tilde{\varphi}(x, y)$ are the generated pseudoamplitude and pseudophase. Here $\mathcal{T}_{\mathrm{LG}}(f_x, f_y)$ is a Laguerre-Gauss transformation in the frequency domain defined as

$$\mathcal{T}_{\mathrm{LG}}(f_x,f_y) = (f_x + jf_y)\exp\left[-\left(f_x^2+f_y^2\right)/\omega^2\right], \tag{2}$$

where ω is a parameter controlling the density of optical vortices in the pseudophase and it is adjusted to a proper value so that the speckle size of the pseudophase representation is close to that of a real speckle. The complex signal representation $\tilde{E}(x, y)$ of a speckle pattern $I(x, y)$ is not unique, for example, one can employ a Riesz transformation [33] or Hilbert transformation [42] in place of the Laguerre-Gauss transformation. This is a classical problem in phase retrieval, and these transformations only exploit the existing information in speckles without introducing any new information [34].

B. Optical vortex motion in simulated speckles

Although the pseudophase cannot reproduce the real phase of a speckle pattern and the fine structure of the optical vortices may not be fully maintained, the spatial-temporal behavior of the optical vortices in the real phase is strictly followed [42,53,63]. To verify whether the motion of the optical vortices in the pseudophase can strictly represent that of the optical vortices in the real phase, we numerically simulate the optical vortices moving in the fluctuating speckle fields. We first generate the evolving speckle fields with different decorrelation rates by superposing a large number of partial waves from random moving scattering centers [30] (more details are given in [64]). The complex representations of the simulated speckle intensity patterns are calculated according to Eq. (1). We then follow the vortex trajectories in both the pseudophase $\tilde{\varphi}(x, y)$ and the real phase $\varphi(x, y)$ and calculate the MSD

$$\langle \Delta r^2(\tau)\rangle = \langle |\vec{r}(t+\tau) - \vec{r}(t)|^2\rangle, \tag{3}$$

where $\vec{r}(t)$ and $\vec{r}(t + \tau)$ are the locations of the optical vortices at times t and $t + \tau$, respectively, and angular brackets represent the ensemble average for all optical vortices. The displacement of the optical vortex is normalized by the speckle size. We compare the MSD of the optical vortices in the real phase, denoted by $\langle \Delta r^2(\tau)\rangle_r$, and the MSD of optical vortices in the corresponding pseudophase, $\langle \Delta r^2(\tau)\rangle_p$, for all simulated speckle sequences and observe an equivalence between the normalized $\langle \Delta r^2(\tau)\rangle_r$ and $\langle \Delta r^2(\tau)\rangle_p$ as shown in Fig. 1(c). This clearly demonstrates that the averaged displacements of the optical vortices in the real phase and the pseudophase of the sequential speckle patterns are the same. We further show that the velocity statistics of the vortices in the real phase and the pseudophase remain consistent [64]. Hence we can explore the motion of the optical vortex in the pseudophase as a replacement for that in the real phase of dynamic speckle sequences.

C. Experimental setup and sample preparation

The optical setup of our experimental system to record time-evolving speckle intensity patterns with the backscattering geometry is given in [64]. To experimentally generate speckle patterns with optical vortices, we focus a He-Ne laser ($\lambda = 632.8$ nm) into a dynamic random sample, composed of light scattering particles, titanium dioxide (TiO_2) microspheres, and optical clear surrounding substrate, a PDMS gel. Light scatterers, TiO_2 nanoparticles (approximately 500 nm in diameter), are randomly mixed in the PDMS matrix with a weight ratio of 1:48. The PDMS (Sylgard 184, Dow Inc.) is prepared by mixing the cross-linking agent and base elastomer in the ratio of 1:5; the resulting reduced scattering coefficient μ_s' of the sample is 24 mm^{-1}. The thickness of the sample is approximately 2 mm, much larger than the mean free path $l = 1/\mu_s'$. The entire process of the PDMS gelation is maintained at 37 °C. The rapidly fluctuating speckle patterns reflected from the sample are captured by a high-speed complementary metal-oxide semiconductor camera (acA2000-340cm, Basler AG) at a frame rate of 300 frames/s. We collect 13 dynamic speckle sequences with 800 speckle images each at intervals of 30 min during the process of PDMS sample gelation. The size of acquired speckle patterns is 416×416 pixels. The complex representations of the experimental speckle intensity patterns are constructed according to Eq. (1). We then track all the optical vortices in the pseudophase of the speckle patterns from creation to annihilation. The locations of the identified vortices over multiple speckle frames trace a separate vortex trail, with the boundary between the new trail and existing trail determined by the average speckle grain size.

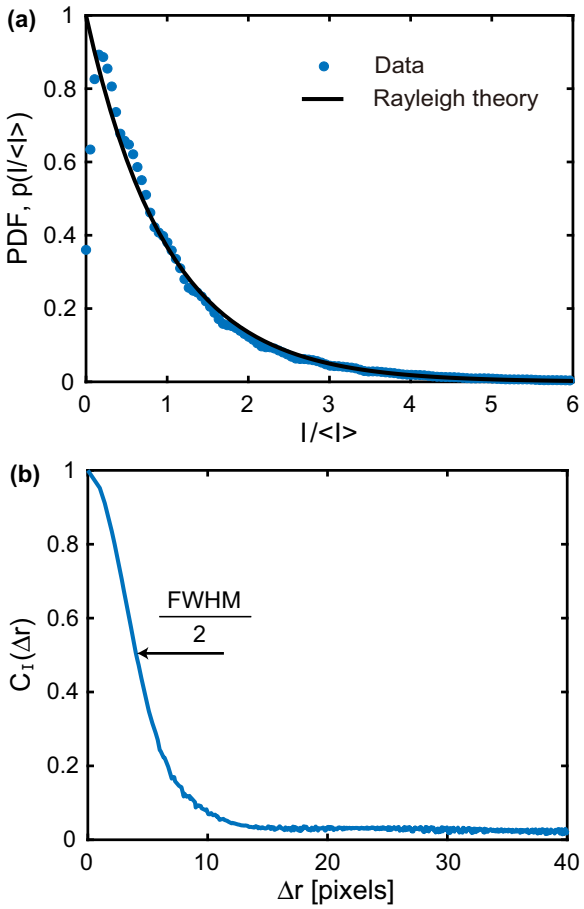

FIG. 2. Statistical properties of speckle patterns. (a) Intensity PDF of the speckle patterns. The PDF of the speckle intensity is consistent with the negative exponential function (black line), demonstrating the Rayleigh statistical property of the speckles. (b) Spatial intensity correlation function of speckle patterns. An ensemble average is performed over 200 speckle frames.

The fully developed Gaussian speckle fields are manifested by the Rayleigh statistics of the recorded speckle intensity [30,65], as the intensity PDF shown in Fig. 2. This means that the phases are uniformly distributed over $[0, 2\pi]$ and the amplitude profiles are independent of the phase profiles. We also specify the speckle grain size or Rayleigh range to identify the characteristic length scales in the speckle pattern by the full width at half maximum of the spatial intensity correlation function

$$C_I(\Delta\mathbf{r}) = \frac{\langle I(\mathbf{r})I(\mathbf{r}+\Delta\mathbf{r})\rangle - \langle I\rangle^2}{\langle I^2\rangle - \langle I\rangle^2}, \tag{4}$$

where the angular brackets denote the ensemble average of speckle intensity. The speckle grain size in our system is about eight camera pixels, well beyond the Nyquist sampling criterion.

III. RESULTS

A. Spatial distribution of optical vortices

We demonstrate that optical vortex trajectories are randomly and uniformly distributed in the entire speckle pattern, as can be seen in Fig. 3. The speckle patterns captured at the initial state of the PDMS curing process decorrelate rapidly; thus the optical vortices possess a considerable proportion of short trails. Here, for simplicity, we show only the trails of optical vortices which can survive over 150 continuous frames. Short trails of optical vortices are also distributed randomly and uniformly in the speckles. Figure 3(a) clearly demonstrates the random spatial-temporal distribution of optical vortices and the random walk of each vortex in finite space. We quantitatively characterize the spatial correlation of optical vortices by calculating the pair and charge correlation functions [51,66]

$$g(r) = \frac{1}{N\rho}\left\langle \sum_{i\neq j} \zeta(r - |\boldsymbol{r}_i - \boldsymbol{r}_j|)\right\rangle, \tag{5}$$

$$g_Q(r) = \frac{1}{N\rho}\left\langle \sum_{i\neq j} \zeta(r - |\boldsymbol{r}_i - \boldsymbol{r}_j|)q_i q_j\right\rangle, \tag{6}$$

where N is the total number of vortices, ρ is the mean density, ζ is the Dirac function, and q is the topological charge of optical vortices. Figure 3(b) shows the correlation statistics $g(r)$ and $g_Q(r)$ for the optical vortices in the pseudophase of speckles. The pair correlation function $g(r)$ returns to unity as the distance r increases, indicating the vortices are spatially independent for $r \to \infty$. When r approaches zero, $g(r)$ is a finite positive value, meaning that we may find two vortices at extremely close positions, for instance, two neighboring vortices with opposite charge which will collide and disappear in a pair. Meanwhile, charge correlation $g_Q(r)$ is almost equivalent to $-g(r)$ for $r \to 0$. These observations reflect representative repulsion between the optical vortices, for instance, two neighboring vortices with the same charge. All the observed results are completely consistent with the characterizations of optical vortices in isotropic random waves [29].

B. Subdiffusion of optical vortices

We explore the stochastic motion of optical vortices in dynamic speckles reflected from the complex viscoelastic PDMS gels. Figure 4 shows the MSDs of optical vortices with the time lag τ at different curing stages $(0, 1, 2, \ldots, 6$ h from the start of gelation) during the PDMS gelation. Throughout the whole PDMS gelation process, all the MSDs increase nonlinearly with time lag τ and demonstrate a power-law dependence of τ, $\langle \Delta r^2(\tau)\rangle \sim \tau^\alpha$. The time lag τ spans nearly three decades for most MSDs from 10^{-3} to 10^0 s. The scaling exponents α for all MSDs are always less than unity, indicating that the optical vortices perform the subdiffusive motion in the speckle fields. At the early curing stages, due to the low viscosity of the PDMS sample, a rapid decorrelation of the speckle patterns is observed, shown in [64]. The corresponding MSD of the optical vortices increases rapidly, suggesting a rapid diffusion of optical vortices. The exponent α decreases from 0.68 to 0.26 with the stiffening of the viscoelastic PDMS sample. For the almost cured PDMS sample, we observe only a slight increment in the MSD curves, which means the vortex motion is tightly restricted.

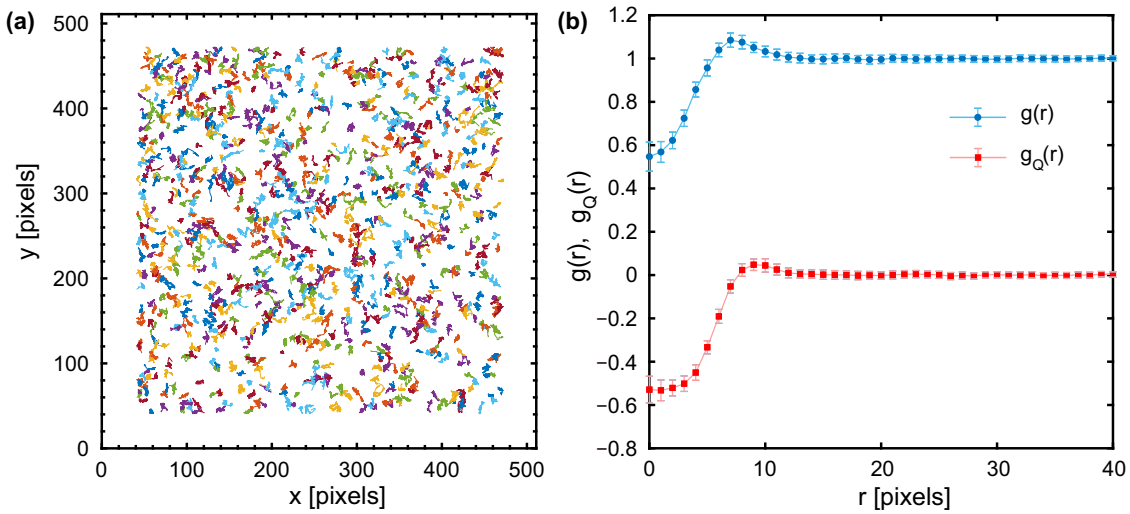

FIG. 3. Spatial distribution of optical vortices. (a) Trajectories of the optical vortices in the pseudophase from dynamic speckle patterns. It is clear that the optical vortex motion yields a stochastic process. (b) Pair (blue circles) and charge (red squares) correlation function of optical vortices as a function of distance r. The error bars correspond to the standard deviations over 200 frames.

C. Underlying mechanism of subdiffusive behavior

Anomalous subdiffusion could be induced by several different mechanisms: a continuous-time random walk (CTRW), obstructed diffusion (OD), and fractional Brownian motion. The CTRW model describes a general process dictated by a sequence of binding-unbinding events in crowded environment and the anomalous diffusion is induced by the broad distribution of the jump lengths and waiting times [67]. In an OD model, a particle encounters a high density of immobile obstacles and the motion of the particle thus becomes subdiffusive with time [68]. For the FBM model, a particle traveling through a semiflexible environment in the presence of both viscous and elastic components moves back and forth in a springlike fashion due to the viscoelastic response. These to-and-fro movements possessing long-time negative correlations in the particle's trajectory, referred to as antipersistent correlation, give rise to the subdiffusive behavior [69,70]. Despite the distinct physical interpretations of these three models, they all lead to a power-law increase of the MSD with time. Therefore, relying solely on the MSD cannot distinguish the underlying mechanism responsible for the subdiffusive behavior [71,72].

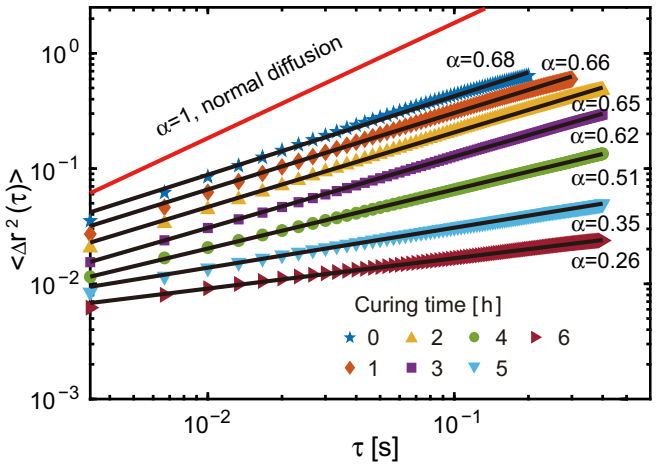

FIG. 4. Subdiffusion of the optical vortices. Shown is a double-logarithmic plot of the MSD for optical vortices in dynamic speckles recorded at different curing times during the PDMS gelation. The data are averaged over 30 000 vortex trajectories with different trail lengths. The black solid lines represent the fits of the MSDs to the power-law relation $\langle \Delta r^2(\tau) \rangle \sim \tau^{\alpha}$, and the corresponding α are listed. The red solid line depicts normal diffusion.

To further the investigation of the subdiffusive behavior of the optical vortices in dynamic speckles, we calculate a diagnostic function [71,72], the velocity autocorrelation function (VAF)

$$C_v^{\delta}(\tau) = \langle \vec{v}(t+\tau) \cdot \vec{v}(t) \rangle, \tag{7}$$

where the averaged velocity $\vec{v}(t) = \frac{1}{\delta}[\vec{r}(t+\delta) - \vec{r}(t)]$ over the time interval $\delta = n \times \Delta T$ s ($n = 1, 2, 3, \ldots, 60$). The smallest increments of time $\Delta T = 1/300$ s, since the number of frames per second of the camera is set to 300 in our experiments. This function describes the degree of correlation between the averaged velocity over two time intervals δ separated by the lag time τ. Figure 5(a) shows the VAFs of the optical vortex motion in random speckles recorded at 3 h after the curing of PDMS started. Each VAF curve in Fig. 5(a) has a different time interval δ. We observe all VAF curves reach a dip into negative values at time δ, indicating the negative correlations of the optical vortex motion in intermediate time. The negative correlation depicts a pushback tendency of the optical vortices in the speckle. This oscillating behavior may arise from the anticorrelation between the vortices [57], which in turn leads to the subdiffusive motion of optical vortices. The observed phenomenon of antipersistent correlation is indicative of FBM, OD, and localization errors of particles, but not the CTRW model [72]. To figure out the origin of the subdiffusion of optical vortices, we examine the VAF as a function of the rescaled time lag τ/δ. We notice that the VAF curves rescaled by the time of the negative dips all collapse to a universal curve as shown in Fig. 5(b). The universal

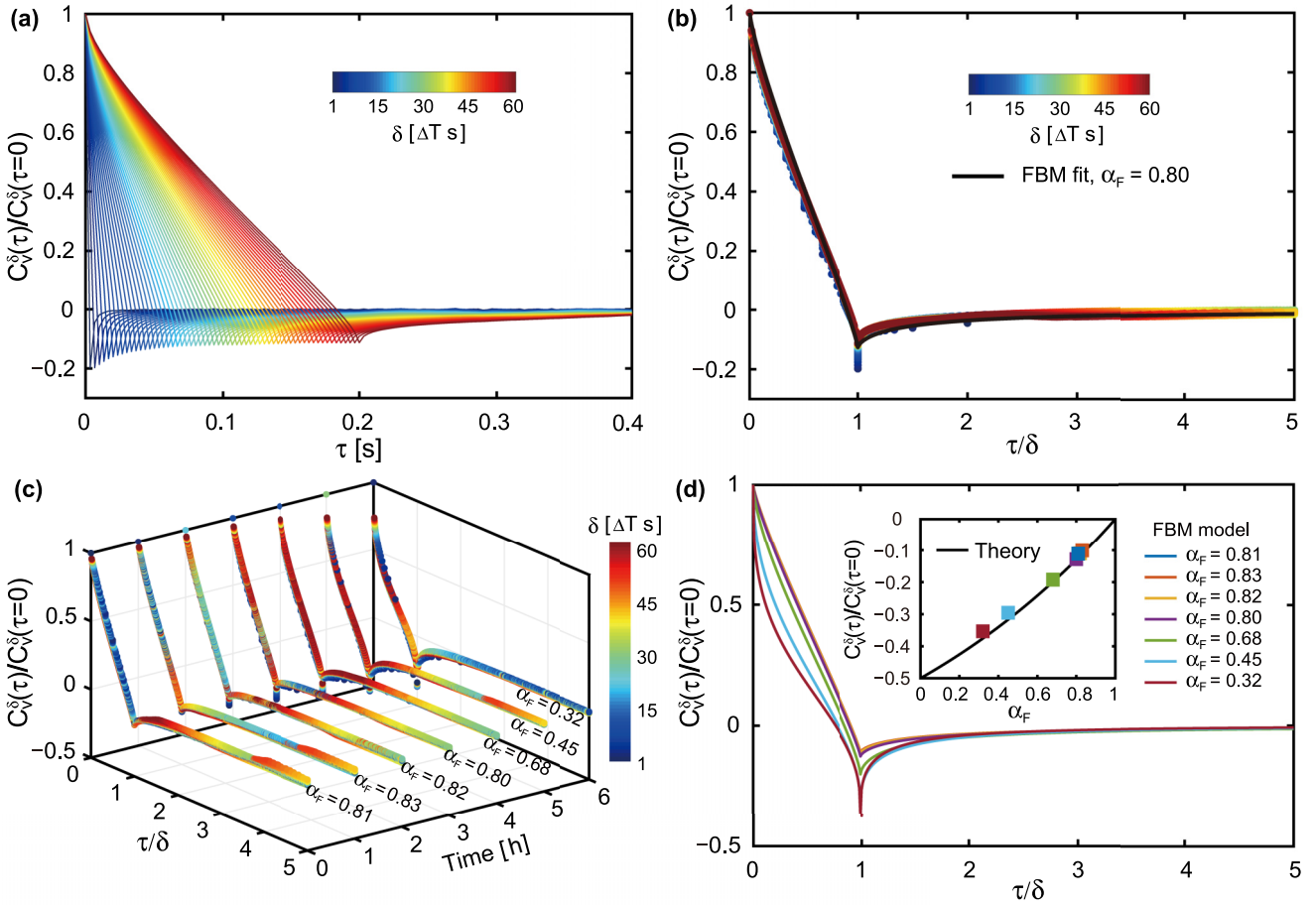

FIG. 5. Velocity autocorrelation function $C_v^\delta(\tau)/C_v^\delta(\tau=0)$ for the anomalous diffusion of optical vortices. The average velocity is calculated at $\delta = n \times \Delta T$ s ($n = 1, 2, 3, \ldots, 60$) (blue to red). The velocity autocorrelation function $C_v^\delta(\tau)/C_v^\delta(\tau=0)$ is plotted against (a) the time lag τ and (b) the rescaled time lag τ/δ. Data are obtained at the time point of 3 h. The black solid line is the FBM fit of the data. (c) The $C_v^\delta(\tau)/C_v^\delta(\tau=0)$ curves acquired at different curing time points versus the rescaled time lag τ/δ. (d) Corresponding FBM fit of the collapsed curves in (c). The scaling exponent α_F ranges from 0.81 to 0.32 as the PDMS sample cures. The inset shows the minimum value of the VAF at τ/δ as a function of the scaling exponent α_F. The solid line is the theoretical prediction with the FBM model.

curve of the rescaled VAF reveals that the motion of optical vortices possesses the striking property of self-similarity, similar patterns at varying temporal scales. More specifically, the velocity correlation of optical vortices remains similar manifestations, although the averaged velocity is calculated over different timescales. The self-similar behaviors of the vortex motion exclude other possible mechanisms of subdiffusion, including the OD model and localization errors in tracking the optical vortex [71–73]. The two properties of self-similarity and antipersistent correlation in the VAF are two signatures of the FBM model; thus we conclude that the optical vortices in dynamic speckles are undergoing anomalous subdiffusive motion in terms of viscoelastic diffusion as FBM.

We also fit the measured velocity autocorrelation function with the theoretical prediction of VAF in the FBM model as [71,74]

$$C_v^\delta(\tau)/C_v^\delta(\tau=0) = \frac{(\eta+1)^{\alpha_F} + |1-\eta|^{\alpha_F} - 2}{2\eta^{\alpha_F}}, \qquad (8)$$

where $1/\eta$ is the rescaled time lag τ/δ. The rescaled VAF shows excellent agreement with Eq. (8), with α_F as the only fitting parameter, as shown in Fig. 5(b). This indicates that the subdiffusive behavior of optical vortices can be well described by the FBM model. Additionally, we calculate the VAF for optical vortices in speckle sequences obtained at different curing stages throughout the PDMS curing process. As shown in Fig. 5(c), all the rescaled VAF curves at different time points show the same tendency of collapsing onto a unique master curve. We fit the collapsed curves to the FBM model and retrieve the scaling exponents α_F. The α_F is proportional to the corresponding α retrieved from the MSD of the optical vortices. Figure 5(d) shows the analytical rescaled $C_v^\delta(\tau)$ in the FBM model. With the PDMS sample gelation, the negative dip of the VAF approaches the theoretical limit (-0.5), which suggests the extreme tight confinement. In the inset we plot the dip values averaged over all time intervals δ at $\tau = \delta$ against the scaling exponent α_F and our experimental results show excellent agreement with the analytical expression in Eq. (8), $C_v^\delta(\tau)/C_v^\delta(\tau = 0) = 2^{\alpha_F - 1} - 1$. This consistency further supports the claimed FBM behavior of optical vortices in dynamic speckles.

D. Non-Gaussianity in FBM

Another significant feature of the normal Brownian diffusion, besides the linear increase in time of the mean-square displacement, is the Gaussian probability distribution of the particle displacements. Brownian motion and the Gaussian process were considered to be intimately tied together according to the central-limit theorem. This connection was enforced by the observations that the particles in pure viscous media undergo Brownian motion accompanied by a Gaussian displacement distribution while certain particle thermal motion displays anomalous diffusion coexisting with a non-Gaussian displacement distribution [14,44,67,75,76]. However, numerous recent reports for different soft materials and biological systems have demonstrated the clear decoupling between the Brownianity and Gaussianity. The intriguing Brownian yet non-Gaussian diffusion has been discovered in crowded colloids [7–9,11], cells, and active matter [5,10,77,78]. The Gaussian but anomalous diffusion has also been identified in dilute solutions [67].

We have demonstrated the optical vortex subdiffusive motion conforming to the FBM through the statistical analysis of the vortex trajectories. In FBM, the PDF of displacements exhibits a Gaussian form

$$P(\Delta x, t) = \frac{1}{\sqrt{4\pi K t^{\alpha}}} \exp\left(-\frac{(\Delta x)^2}{4Kt^{\alpha}}\right). \tag{9}$$

The optical vortex thus may perform a Gaussian anomalous diffusion. However, we further study the probability distribution of optical vortex displacements and find obvious deviations from the Gaussian distribution. As shown in Fig. 6, the PDFs of optical vortex transverse displacements Δx at different lag time τ are perfectly fit to the Gaussian distributions only at small displacements. At large displacements, the PDFs deviate from the Gaussian distributions and transit to the heavy exponential tails quickly. The PDFs with the sharp transitions from Gaussian distributions to exponential tails are similar to the PDFs of the Brownian yet non-Gaussian diffusion. By comparing Figs. 6(a) and 6(b), we also notice that the PDFs possess a narrower width at the later gelling stage [Fig. 6(b)] than the PDFs at an early gelling stage [Fig. 6(a)]. The reason is that, at the later gelling stage, the light scattering particles move slowly in the media with higher viscoelastic modulus. As a result, the laser speckles fluctuate slowly and the optical vortices move slowly. The underlying physical mechanism of the non-Gaussian behavior in normal or anomalous diffusion is still highly debated [44,79–83]. The discovered non-Gaussian behavior of optical vortex subdiffusion may also enrich the understanding of this general phenomenon.

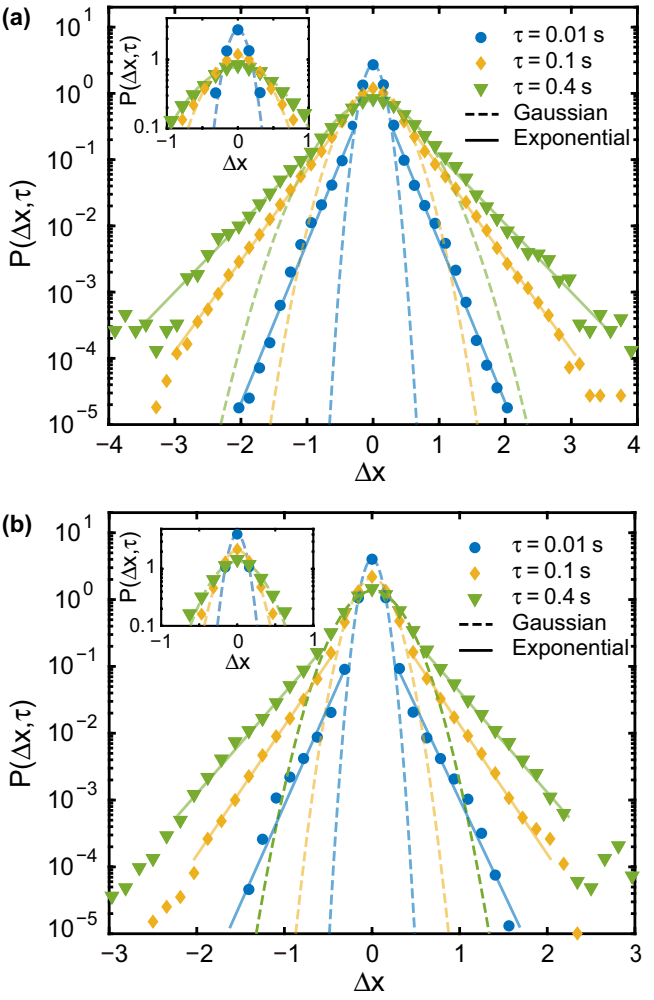

FIG. 6. Non-Gaussian behavior of optical vortices. (a) Displacement PDFs over six orders of magnitude plotted against the displacement Δx at the initial state of PDMS gelation, at time lags of 0.01, 0.05, 0.1, 0.2, and 0.4 s. The dashed lines represent the Gaussian distribution and the solid lines show the exponential distribution at corresponding time lags. The inset shows a log-linear plot of the same data at small Δx values. (b) Data are obtained at the PDMS curing stage of 3 h after curing starts.

IV. DISCUSSION

The subdiffusive behavior of optical vortices and the constrained motion with the viscoelasticity resemble those of particles in viscoelastic media. Single- or multiple-particle tracking is a well-established technique for evaluating the dynamic properties of complex systems including molecular transport and microrheological properties of soft materials. Our results suggest an optical microrheology which tracks the optical vortices rather than the exogenous probe particles to evaluate the viscoelasticity of turbid media. We conceptually prove this microrheology approach by exploring the relation between the optical vortex dynamics and the viscoelasticity of the sample. The frequency-dependent viscoelastic modulus, $|G^*(\nu)|$ from 1 to 100 Hz, of the PDMS sample is measured with a conventional mechanical rheometer while the speckle sequences are recording. During the gelation, the viscoelastic modulus of PDMS is increasing due to the formation of cross-linking structures [64]. In Fig. 7 we plot the MSD of the optical vortices $\langle \Delta r^2(\tau) \rangle$ versus the viscoelastic modulus of the sample $|G^*(\nu)|$ at $\nu = 5$ Hz, while $\tau = 1/\nu$ at different curing times. We clearly observe a strong inverse linear relation between $\langle \Delta r^2(\tau) \rangle$ and $|G^*(\nu)|$ in logarithmic scale,

$$|G^*(\nu)| \propto \frac{1}{[\langle \Delta r^2(\tau) \rangle]^k}, \tag{10}$$

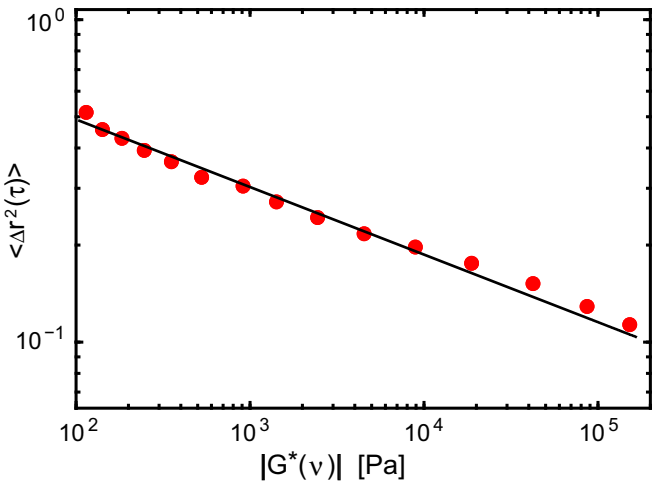

FIG. 7. Double-logarithmic plot of the MSD of the optical vortices $\langle \Delta r^2(\tau) \rangle$ versus the corresponding viscoelastic modulus of the PDMS sample $|G^*(\nu)|$ at $\nu = 5$ Hz, while $\tau = 1/\nu$. The black line represents the fit with Eq. (10) ($r = 0.99$, $p < 0.0001$).

where k represents the slope of the linear regression line when plotted on a double-logarithmic coordinate system. This relation indicates that the optical vortex motion is sensitive to the viscoelastic properties of the sample. More investigations to explore the quantitative relation between the viscoelastic modulus and the motion of optical vortices, aiming to establish the optical-vortex-tracking-based microrheological approach, are left for future work.

Vortices or phase singularities are present not only in wave fields but also in many different physical systems, where they are better known as quantized vortices in superfluids [12,16,84] or topological defects in liquid crystals and even in cell membranes [17,85,86]. The analogy between the underlying physics that governs the vortices in different systems has been well recognized for decades. For example, the wave coherence in random wave fields has been admitted to be an analogy to the quantum coherence in turbulent superfluids [22,43]. Hence the above analysis of the optical vortex motion may also contribute to the investigation into the collective dynamics of other vortices [22].

V. CONCLUSION

We have presented direct experimental evidence of the anomalous diffusion of optical vortices in viscoelastic media. We found that the subdiffusive motion of optical vortices clearly shows two crucial features, self-similarity and antipersistence, which can only be interpreted by the fractional Brownian motion model. In addition, we observed a robust non-Gaussian behavior in the probability distribution of the optical vortex displacements, which is directly contradicted by the Gaussian property of the fractional Brownian motion. We also found the extent to which the optical vortex subdiffusion can be tuned by the changes in the viscoelasticity of the light scattering media. The findings of anomalous yet non-Gaussian diffusion of optical vortices not only enrich our understanding of the relation between Brownianity and Gaussianity [9,11,87], but also extend the knowledge of anomalous diffusion of vortices from systems with rest masses like fluids or superfluids [16,22,43] to the massless systems like the phase or polarization of random light fields [28,88–90]. The similarity between the subdiffusion of optical vortices in speckle fields from turbid viscoelastic media and the particle subdiffusion in the viscoelastic environment strongly suggests an optical-vortex-tracking-based microrheological approach, particularly for turbid soft matter or biological tissues, as a counterpart of single- or multiple-particle-tracking microrheology [91].

ACKNOWLEDGMENTS

We acknowledge the National Natural Science Foundation of China (No. 82227805) and Shccig-Qinling Program (SZYJY20230117).

[1] C. W. Gardiner, *Stochastic Methods: A Handbook for the Natural and Social Sciences* (Springer, Berlin, 2009).
[2] D. Molina-Garcia, T. Sandev, H. Safdari, G. Pagnini, A. Chechkin, and R. Metzler, Crossover from anomalous to normal diffusion, New J. Phys. **20**, 103027 (2018).
[3] R. Metzler, Brownian motion and beyond: First-passage, power spectrum, non-Gaussianity, and anomalous diffusion, J. Stat. Mech. (2019) 114003.
[4] A. Lampo, M. A. García March, and M. Lewenstein, *Quantum Brownian Motion Revisited: Extensions and Applications*, 1st ed. (Springer, Cham, 2019).
[5] K. Kanazawa, T. G. Sano, A. Cairoli, and A. Baule, Loopy Lévy flights enhance tracer diffusion in active suspensions, Nature (London) **579**, 364 (2020).
[6] E. Fonda, K. R. Sreenivasan, and D. P. Lathrop, Reconnection scaling in quantum fluids, Proc. Natl. Acad. Sci. USA **116**, 1924 (2019).
[7] B. Wang, S. M. Anthony, C. B. Sung, and S. Granick, Anomalous yet Brownian, Proc. Natl. Acad. Sci. USA **106**, 15160 (2009).
[8] J. Guan, B. Wang, and S. Granick, Even hard-sphere colloidal suspensions display Fickian yet non-Gaussian diffusion, ACS Nano **8**, 3331 (2014).
[9] R. Pastore, A. Ciarlo, G. Pesce, F. Greco, and A. Sasso, Rapid Fickian yet non-Gaussian diffusion after subdiffusion, Phys. Rev. Lett. **126**, 158003 (2021).
[10] F. Guzmán-Lastra, H. Löwen, and A. J. Mathijssen, Active carpets drive non-equilibrium diffusion and enhanced molecular fluxes, Nat. Commun. **12**, 1906 (2021).
[11] F. Rusciano, R. Pastore, and F. Greco, Universal evolution of Fickian non-Gaussian diffusion in two- and three-dimensional glass-forming liquids, Int. J. Mol. Sci. **24**, 7871 (2023).
[12] A. L. Fetter, Vortices and dynamics in trapped Bose-Einstein condensates, J. Low Temp. Phys. **161**, 445 (2010).

[13] S. Song, S. J. Park, M. Kim, J. S. Kim, B. J. Sung, S. Lee, J. H. Kim, and J. Sung, Transport dynamics of complex fluids, Proc. Natl. Acad. Sci. USA **116**, 12733 (2019).
[14] F. Höfling and T. Franosch, Anomalous transport in the crowded world of biological cells, Rep. Prog. Phys. **76**, 046602 (2013).
[15] K. L. Chong, J. Q. Shi, G. Y. Ding, S. S. Ding, H. Y. Lu, J. Q. Zhong, and K. Q. Xia, Vortices as Brownian particles in turbulent flows, Sci. Adv. **6**, eaaz1110 (2020).
[16] Y. Tang, S. Bao, and W. Guo, Superdiffusion of quantized vortices uncovering scaling laws in quantum turbulence, Proc. Natl. Acad. Sci. USA **118**, e2021957118 (2021).
[17] T. H. Tan, J. Liu, P. W. Miller, M. Tekant, J. Dunkel, and N. Fakhri, Topological turbulence in the membrane of a living cell, Nat. Phys. **16**, 657 (2020).
[18] X. Huang, W. Xu, J. Liang, K. Takagaki, X. Gao, and J.-Y. Wu, Spiral wave dynamics in neocortex, Neuron **68**, 978 (2010).
[19] J. Christoph, M. Chebbok, C. Richter, J. Schröder-Schetelig, P. Bittihn, S. Stein, I. Uzelac, F. H. Fenton, G. Hasenfuß, R. F. Gilmour, and S. Luther, Electromechanical vortex filaments during cardiac fibrillation, Nature (London) **555**, 667 (2018).
[20] R. Zhang, S. A. Redford, P. V. Ruijgrok, N. Kumar, A. Mozaffari, S. Zemsky, A. R. Dinner, V. Vitelli, Z. Bryant, M. L. Gardel, and J. J. de Pablo, Spatiotemporal control of liquid crystal structure and dynamics through activity patterning, Nat. Mater. **20**, 875 (2021).
[21] K. Copenhagen, R. Alert, N. S. Wingreen, and J. W. Shaevitz, Topological defects promote layer formation in *Myxococcus xanthus* colonies, Nat. Phys. **17**, 211 (2021).
[22] S. N. Alperin, A. L. Grotelueschen, and M. E. Siemens, Quantum turbulent structure in light, Phys. Rev. Lett. **122**, 044301 (2019).
[23] J. M. Andersen, A. A. Voitiv, M. E. Siemens, and M. T. Lusk, Hydrodynamics of noncircular vortices in beams of light and other two-dimensional fluids, Phys. Rev. A **104**, 033520 (2021).
[24] D. Rozas, Z. S. Sacks, and G. A. Swartzlander, Experimental observation of fluidlike motion of optical vortices, Phys. Rev. Lett. **79**, 3399 (1997).
[25] P. Wiegmann and A. G. Abanov, Anomalous hydrodynamics of two-dimensional vortex fluids, Phys. Rev. Lett. **113**, 034501 (2014).
[26] J. Gateau, F. Claude, G. Tessier, and M. Guillon, Topological transformations of speckles, Optica **6**, 914 (2019).
[27] Z. Zhang, F. Li, G. Malpuech, Y. Zhang, O. Bleu, S. Koniakhin, C. Li, Y. Zhang, M. Xiao, and D. D. Solnyshkov, Particlelike behavior of topological defects in linear wave packets in photonic graphene, Phys. Rev. Lett. **122**, 233905 (2019).
[28] D. Sugic, R. Droop, E. Otte, D. Ehrmanntraut, F. Nori, J. Ruostekoski, C. Denz, and M. R. Dennis, Particle-like topologies in light, Nat. Commun. **12**, 6785 (2021).
[29] M. V. Berry and M. R. Dennis, Phase singularities in isotropic random waves, Proc. R. Soc. A **456**, 2059 (2000).
[30] J. W. Goodman, *Speckle Phenomena in Optics: Theory and Applications* (Roberts, Greenwood Village, 2007).
[31] S. Zhang, B. Hu, P. Sebbah, and A. Z. Genack, Speckle evolution of diffusive and localized waves, Phys. Rev. Lett. **99**, 063902 (2007).
[32] S. Zhang, Y. Lockerman, and A. Z. Genack, Mesoscopic speckle, Phys. Rev. E **82**, 051114 (2010).
[33] W. Wang, T. Yokozeki, R. Ishijima, A. Wada, Y. Miyamoto, M. Takeda, and S. G. Hanson, Optical vortex metrology for nanometric speckle displacement measurement, Opt. Express **14**, 120 (2006).
[34] G. H. Sendra, H. J. Rabal, R. Arizaga, and M. Trivi, Vortex analysis in dynamic speckle images, J. Opt. Soc. Am. A **26**, 2634 (2009).
[35] X. Cheng, Y. Lockerman, and A. Z. Genack, Phase singularity diffusion, Opt. Lett. **39**, 3348 (2014).
[36] W. Wang, Y. Qiao, R. Ishijima, T. Yokozeki, D. Honda, A. Matsuda, S. G. Hanson, and M. Takeda, Constellation of phase singularities in a speckle-like pattern for optical vortex metrology applied to biological kinematic analysis, Opt. Express **16**, 13908 (2008).
[37] N. Bender, M. Sun, H. Yilmaz, J. Bewersdorf, and H. Cao, Circumventing the optical diffraction limit with customized speckles, Optica **8**, 122 (2021).
[38] J. Gong, Y. Zhang, H. Zhang, Q. Li, G. Ren, W. Lu, and J. Wang, Evaluation of blood coagulation by optical vortex tracking, Sensors **22**, 4793 (2022).
[39] K. O'Holleran, M. R. Dennis, F. Flossmann, and M. J. Padgett, Fractality of light's darkness, Phys. Rev. Lett. **100**, 053902 (2008).
[40] K. O'Holleran, M. R. Dennis, and M. J. Padgett, Topology of light's darkness, Phys. Rev. Lett. **102**, 143902 (2009).
[41] L. De Angelis and L. Kuipers, Effective pair-interaction of phase singularities in random waves, Opt. Lett. **46**, 2734 (2021).
[42] S. J. Kirkpatrick, K. Khaksari, D. Thomas, and D. D. Duncan, Optical vortex behavior in dynamic speckle fields, J. Biomed. Opt. **17**, 050504 (2012).
[43] I. Carusotto and C. Ciuti, Quantum fluids of light, Rev. Mod. Phys. **85**, 299 (2013).
[44] R. Metzler, Gaussianity fair: The riddle of anomalous yet non-Gaussian diffusion, Biophys. J. **112**, 413 (2017).
[45] I. Freund and N. Shvartsman, Wave-field phase singularities: The sign principle, Phys. Rev. A **50**, 5164 (1994).
[46] I. Freund, N. Shvartsman, and V. Freilikher, Optical dislocation networks in highly random media, Opt. Commun. **101**, 247 (1993).
[47] N. Shvartsman and I. Freund, Speckle spots ride phase saddles sidesaddle, Opt. Commun. **117**, 228 (1995).
[48] A. A. Voitiv, J. M. Andersen, P. C. Ford, M. T. Lusk, and M. E. Siemens, Hydrodynamics explanation for the splitting of higher-charge optical vortices, Opt. Lett. **47**, 1391 (2022).
[49] I. Freund, Optical vortex trajectories, Opt. Commun. **181**, 19 (2000).
[50] V. N. Gorshkov, A. N. Kononenko, and M. S. Soskin, Topology of optical vortices spontaneous birth, Proc. SPIE **4607**, 13 (2002).
[51] L. De Angelis, F. Alpeggiani, A. Di Falco, and L. Kuipers, Spatial distribution of phase singularities in optical random vector waves, Phys. Rev. Lett. **117**, 093901 (2016).
[52] L. De Angelis, F. Alpeggiani, A. Di Falco, and L. Kuipers, Persistence and lifelong fidelity of phase singularities in optical random waves, Phys. Rev. Lett. **119**, 203903 (2017).
[53] M. Szatkowski, E. Burnecka, H. Dyła, and J. Masajada, Optical vortex tracking algorithm based on the Laguerre-Gaussian transform, Opt. Express **30**, 17451 (2022).
[54] E. Cuche, F. Bevilacqua, and C. Depeursinge, Digital holography for quantitative phase-contrast imaging, Opt. Lett. **24**, 291 (1999).

[55] P. Etchepareborda, A. Bianchetti, F. E. Veiras, A. L. Vadnjal, A. Federico, and G. H. Kaufmann, Comparison of real-time phase-reconstruction methods in temporal speckle-pattern interferometry, Appl. Opt. **54**, 7663 (2015).

[56] C. Zuo, J. Li, J. Sun, Y. Fan, J. Zhang, L. Lu, R. Zhang, B. Wang, L. Huang, and Q. Chen, Transport of intensity equation: A tutorial, Opt. Lasers Eng. **135**, 106187 (2020).

[57] N. Shvartsman and I. Freund, Vortices in random wave fields: Nearest neighbor anticorrelations, Phys. Rev. Lett. **72**, 1008 (1994).

[58] M. Pascucci, G. Tessier, V. Emiliani, and M. Guillon, Superresolution imaging of optical vortices in a speckle pattern, Phys. Rev. Lett. **116**, 093904 (2016).

[59] J. W. Goodman, *Statistical Optics*, 2nd ed. (Wiley, Hoboken, 2015).

[60] W. Wang, T. Yokozeki, R. Ishijima, M. Takeda, and S. G. Hanson, Optical vortex metrology based on the core structures of phase singularities in Laguerre-Gauss transform of a speckle pattern, Opt. Express **14**, 10195 (2006).

[61] Y. Qiao, W. Wang, N. Minematsu, J. Liu, M. Takeda, and X. Tang, A theory of phase singularities for image representation and its applications to object tracking and image matching, IEEE Trans. Image Process. **18**, 2153 (2009).

[62] S. C. Pei, C. L. Liu, and Y. C. Lai, Discrete Laguerre Gaussian transforms and their applications, IEEE Trans. Signal Process. **64**, 3156 (2016).

[63] F. E. Veiras, A. L. Vadnjal, P. Etchepareborda, A. Bianchetti, A. Federico, and G. H. Kaufmann, Comparisons between singularities of pseudophase and speckle phase using binary diffusers in optical vortex metrology, Opt. Eng. **55**, 121712 (2016).

[64] See Supplemental Material at http://link.aps.org/supplemental/10.1103/PhysRevE.109.024111 for additional information, including the simulation of dynamic speckle fields, the temporal decorrelation of experimental dynamic speckles, pure diffusion of optical vortices, and the experimental setup.

[65] N. Bender, H. Yilmaz, Y. Bromberg, and H. Cao, Customizing speckle intensity statistics, Optica **5**, 595 (2018).

[66] L. De Angelis, T. Bauer, F. Alpeggiani, and L. Kuipers, Index-symmetry breaking of polarization vortices in 2D random vector waves, Optica **6**, 1237 (2019).

[67] R. Metzler and J. Klafter, The random walk's guide to anomalous diffusion: A fractional dynamics approach, Phys. Rep. **339**, 1 (2000).

[68] M. J. Saxton, Anomalous diffusion due to obstacles: A Monte Carlo study, Biophys. J. **66**, 394 (1994).

[69] B. B. Mandelbrot and J. W. V. Ness, Fractional Brownian motions, fractional noises and applications, SIAM Rev. **10**, 422 (1968).

[70] W. Wang, A. G. Cherstvy, H. Kantz, R. Metzler, and I. M. Sokolov, Time averaging and emerging nonergodicity upon resetting of fractional Brownian motion and heterogeneous diffusion processes, Phys. Rev. E **104**, 024105 (2021).

[71] S. C. Weber, A. J. Spakowitz, and J. A. Theriot, Bacterial chromosomal loci move subdiffusively through a viscoelastic cytoplasm, Phys. Rev. Lett. **104**, 238102 (2010).

[72] S. C. Weber, M. A. Thompson, W. E. Moerner, A. J. Spakowitz, and J. A. Theriot, Analytical tools to distinguish the effects of localization error, confinement, and medium elasticity on the velocity autocorrelation function, Biophys. J. **102**, 2443 (2012).

[73] I. Goychuk and T. Pöschel, Fingerprints of viscoelastic subdiffusion in random environments: Revisiting some experimental data and their interpretations, Phys. Rev. E **104**, 034125 (2021).

[74] S. Burov, J. H. Jeon, R. Metzler, and E. Barkai, Single particle tracking in systems showing anomalous diffusion: The role of weak ergodicity breaking, Phys. Chem. Chem. Phys. **13**, 1800 (2011).

[75] J. H. Jeon, M. Javanainen, H. Martinez-Seara, R. Metzler, and I. Vattulainen, Protein crowding in lipid bilayers gives rise to non-Gaussian anomalous lateral diffusion of phospholipids and proteins, Phys. Rev. X **6**, 021006 (2016).

[76] T. J. Lampo, S. Stylianidou, M. P. Backlund, P. A. Wiggins, and A. J. Spakowitz, Cytoplasmic RNA-protein particles exhibit non-Gaussian subdiffusive behavior, Biophys. J. **112**, 532 (2017).

[77] H. Kurtuldu, J. S. Guasto, K. A. Johnson, and J. P. Gollub, Enhancement of biomixing by swimming algal cells in two-dimensional films, Proc. Natl. Acad. Sci. USA **108**, 10391 (2011).

[78] W. He, H. Song, Y. Su, L. Geng, B. J. Ackerson, H. B. Peng, and P. Tong, Dynamic heterogeneity and non-Gaussian statistics for acetylcholine receptors on live cell membrane, Nat. Commun. **7**, 11701 (2016).

[79] B. Wang, J. Kuo, S. C. Bae, and S. Granick, When Brownian diffusion is not Gaussian, Nat. Mater. **11**, 481 (2012).

[80] M. V. Chubynsky and G. W. Slater, Diffusing diffusivity: A model for anomalous, yet Brownian, diffusion, Phys. Rev. Lett. **113**, 098302 (2014).

[81] V. Sposini, A. V. Chechkin, F. Seno, G. Pagnini, and R. Metzler, Random diffusivity from stochastic equations: Comparison of two models for Brownian yet non-Gaussian diffusion, New J. Phys. **20**, 043044 (2018).

[82] R. Metzler, Superstatistics and non-Gaussian diffusion, Eur. Phys. J.: Spec. Top. **229**, 711 (2020).

[83] I. Chakraborty and Y. Roichman, Disorder-induced Fickian, yet non-Gaussian diffusion in heterogeneous media, Phys. Rev. Res. **2**, 022020(R) (2020).

[84] G. L. Eyink and K. R. Sreenivasan, Onsager and the theory of hydrodynamic turbulence, Rev. Mod. Phys. **78**, 87 (2006).

[85] M. Kleman, Defects in liquid crystals, Rep. Prog. Phys. **52**, 555 (1989).

[86] E. Brasselet and C. Loussert, Electrically controlled topological defects in liquid crystals as tunable spin-orbit encoders for photons, Opt. Lett. **36**, 719 (2011).

[87] A. G. Cherstvy, S. Thapa, C. E. Wagner, and R. Metzler, Non-Gaussian, non-ergodic, and non-Fickian diffusion of tracers in mucin hydrogels, Soft Matter **15**, 2526 (2019).

[88] G. Gbur, Fractional vortex Hilbert's hotel, Optica **3**, 222 (2016).

[89] R. Chriki, S. Smartsev, D. Eger, O. Firstenberg, and N. Davidson, Coherent diffusion of partial spatial coherence, Optica **6**, 1406 (2019).

[90] K. A. Sitnik, S. Alyatkin, J. D. Töpfer, I. Gnusov, T. Cookson, H. Sigurdsson, and P. G. Lagoudakis, Spontaneous formation of time-periodic vortex crystals in nonlinear fluids of light, Phys. Rev. Lett. **128**, 237402 (2022).

[91] R. Pastore, A. Ciarlo, G. Pesce, A. Sasso, and F. Greco, A model-system of Fickian yet non-Gaussian diffusion: Light patterns in place of complex matter, Soft Matter **18**, 351 (2022).